05,08,10

# Local states of a synthetic ferrimagnet induced by the field of ferromagnetic particles on its surface

© E.I. Kunitsyna, R.B. Morgunov¶

Federal Research Center of Problems of Chemical Physics and Medicinal Chemistry RAS, Chernogolovka, Russia

¶ E-mail: spintronics2022@yandex.ru

*Received August 19, 2024*
*Revised November 18, 2024*
*Accepted November 26, 2024*

The magnetization reversal of local regions of CoFeB layers in a CoFeB/Ta/CoFeB heterostructure consisting of two ferromagnetic layers separated by a non-magnetic material under the action of a single ferromagnetic nanoparticle on its surface was studied by micromagnetic modeling. The modeling results demonstrate many unusual states with non-uniform magnetization distribution in ferromagnetic films. This is of interest for accurate measurements of the concentration of nanoparticles or magnetically labeled objects deposited on the surface of ferromagnetic sensors based on heterostructures with giant magnetoresistance.

**Keywords:** nanoparticles, micromagnetic modeling, heterostructures, magnetoresistive sensors, spin valve, perpendicular anisotropy.

DOI: 10.61011/PSS.2024.12.60212.216

## 1. Introduction

One of the spin valve applications involves the fabrication of a platform whose resistance is sensitive to the presence of ferromagnetic or ferromagnetic-particle-labeled biological objects (cells) on its surface [1–3]. General concept of such sensors, that are necessary for medical and biological applications, is in that local remagnetization of ferromagnetic sensor layers exposed to a ferromagnetic particle field leads to a change in the local magnetoresistance. Therefore, soft-magnetic metals that has already shown their ability to provide high magnetoresistance such as CoFeB/Ta/CoFeB are chosen for such sensors [4]. However, details of remagnetization of such structures in a nonuniform particle field are complex and often affect the proportion between the signal and number of particles. In particular, overlapping of local remagnetized areas under particles at high nanoparticle concentrations leads to difficult sensor conditions degrading its sensitivity and linearity. But even a single isolated ferromagnetic particle induces complex magnetization distributions of layers interacting with each other in a two-layer heterostructure. Unlike a single layer, where a ferromagnetic particle creates easily predictable magnetization directions, the same problem becomes difficult in multilayer systems, which prevents from using intuitive and judgmental approaches. Nonuniform field of ferromagnetic particles switches four possible states of a double-layer sensor (↑↑, ↑↓, ↓↑, ↓↓), where arrows show the layer magnetization directions) inducing different states at different distances from the particle. Magnetic field components perpendicular and parallel to the structure may also induce other intermediate states that don't coincide with the four mentioned above stable states in a perpendicular magnetic field.

There are considerable experimental difficulties in measuring local magnetization of ferromagnetic sensor layers in the vicinity of the nanoparticle. A surface-scanning atomic magnetic force microscope (MFM) is generally used for this. In [5,6], remagnetized state of the ferromagnetic film under the particle was detected in structures with perpendicular magnetization in the form of a kind of „magnetic shadow" induced by the particle under itself. MFM resolution is insufficient to detect various types of states because the difference between their magnetizations is small and the sensor relief is usually insufficiently smooth to maintain a constant close distance between the magnetic cantilever and surface. In addition, magnetic fields of the cantilever, particle itself and magnetized areas of the film are overlapped preventing from detecting sharp area boundaries. In these conditions, modeling of areas remagnetized under the particle using object-oriented programming of micromagnetic states (OOMMF, muMag, etc.) is essential. This provides better understanding and interpreting of experimental data and calculation of expected magnetizations of various surface areas. Study [6] describes modeling examples and comparison with experimental data for a system consisting of nanoparticles and a double-layer synthetic perpendicular-anisotropy ferrimagnet. This work is attempting to develop the description of remagnetized area of a double-layer CoFeB/Ta/CoFeB sensor through modeling.

The objective of our study is to calculate magnetization and magnetoresistance distributions for a single CoFeB layer and synthetic CoFeB/Ta/CoFeB perpendicular-anisotropy

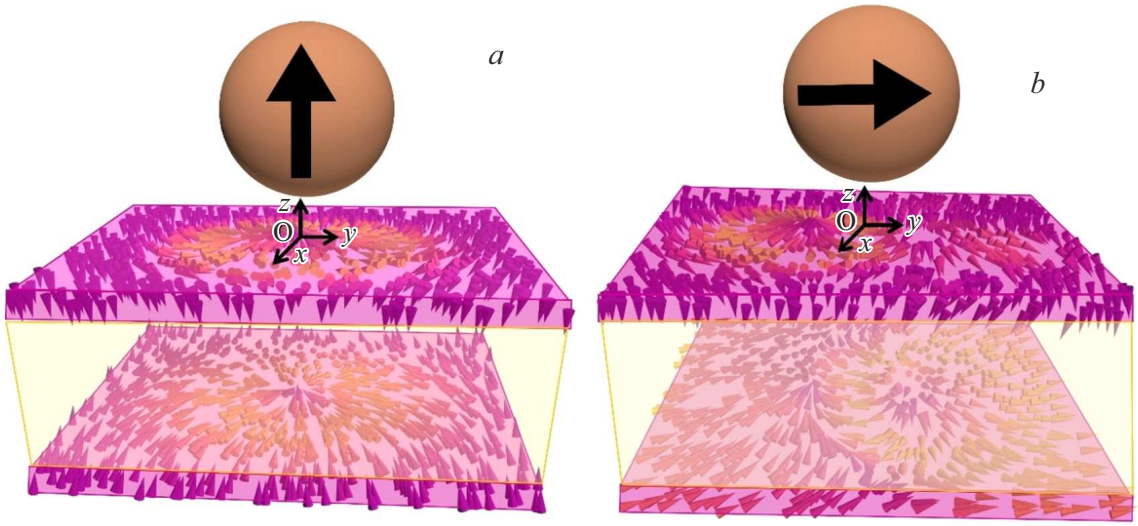


**Figure 1.** Schematic diagrams of CoFeB/Ta/CoFeB platform **II** exposed to the external uniform field **H** and nanoparticle scattering field $\mathbf{H_{dip}}$ with the magnetic moment $\mathbf{m_p}$. Field **H** is applied at the angle$\theta = 0^\circ$ (*a*) and $90^\circ$ (*b*) to the normal **n** (co-directional to the *z* axis).

ferrimagnet in the presence of ferromagnetic nanoparticles on the surface.

## 2. Experimental methods and samples

Parameters of real heterostructures with the perpendicular type of anisotropy will be used for modeling. The experiments used two types of samples: a single-layer MgO(2.5 nm)/CoFeB(0.8 nm)/MgO(2.5 nm)/Ta(0.75 nm) heterostructure (platform **I**) and double-layer gO(2.5 nm)/CoFeB(1.1 nm)/Ta(0.75 nm)/CoFeB(0.8 nm)/MgO(2.5 nm)/Ta(0.75 nm) heterostructure (platform **II**) (Figure 1). The samples were grown on undoped GaAs (001) substrates. The first MgO layer is a buffer layer. For details of growing such structures and of their magnetic properties see [7,8]. The samples consisted of $3 \times 4.5 \times 0.1$ mm wafers.

For the purpose of our study, it was important that the particles were single-domain and assumed as a uniformly magnetized sphere during calculation. $Fe_3O_4$ coated Fe nanoparticles were produced by decomposition of a previously prepared Fe oleate complex at a high temperature in squalene. According to the previous studies [5,6], the $Fe/Fe_3O_4$ particles are superparamagnetic at room temperature with the saturation magnetization $M_S = 101\,\mathrm{A \cdot m^2/kg}$ at 5 K, $M_S = 95\,\mathrm{A \cdot m^2/kg}$ at 300 K and magnetic anisotropy constant $K_{\mathrm{eff}} = 1.6 \cdot 10^5\,\mathrm{J/m^3}$ at 5 K. Typical oxide shell thickness is about 3 nm. At 5 K the coercive force of nanoparticles is equal to $H_C = 440$ Oe. Exchange interaction between the core and shell may be neglected. But the presence of the shell ensures individual magnetization stability of a nanoparticle and prevents occurrence of a domain structure in it.

Particles were dissolved in cyclohexane and separated in an ultrasound bath. About $\sim 0.1$ ml of liquid containing nanoparticle clusters was applied to the platform surface. A silicon wafer was used as test sample platforms, and images produced on this wafer were compared with re-magnetized area images on ferromagnetic platforms **I** or **II**. After drying out of the surface, relatively good adhesion between the particle and sample surface was provided to ensure placement of the sample into the magnetometer. magnetization was measured using the Quantum design MPMS XL SQUID magnetometer.

Surface morphology and magnetic force gradient distribution on the sample surface were studied by the atomic force microscopy (AFM) and magnetic force microscopy (MFM) methods, respectively. Magnetic relief images in the studied samples were obtained using the Aura Integra (NT MDT) atomic-force microscope without a magnetic field. A standard MFM_LM series silicon cantilever coated with a thin CoCr film with a coercive force of about 400 Oe was used. A tapping-lift scanning mode was used for all experiments. Force constant and resonance frequency of the cantilever were equal to 5 N/m and 63 kOe, respectively. For the first path, the cantilever was used in the tapping-lift mode and measured physical particle sizes with accuracy to the Van der Waals radius, i. e. the distance between the cantilever and probe was close to the cantilever vibrations. For the second path, the probe was removed from the platform surface at $h = 50$ nm and the magnetic dipole force gradient between the particle and probe was measured.

Images of microparticles on Si were made by the SUPRA 25 (Zeiss) scanning electron microscope (SEM).

OOMMF (Object Oriented Micromagnetic Framework) was used for modeling the single-layer CoFeB platform (platform **I**) and (CoFeB/Ta/CoFeB) platform **II**. The program code is based on the solution of a system of Landau-Lifshitz-Hilbert differential equations for spin relaxation.

For modeling platform **I**, horizontal dimensions of the platform $1500 \times 1500$ nm and sampling cell dimensions $5 \times 5 \times 0.3$ nm were used. Magnetic parameters for platform **I** were taken equal to those for the top ferromagnetic layer of platform **II** that were calculated earlier in [9]: saturation magnetization $M_s = 952$ emu/cm$^3$, magnetocrystalline anisotropy constant $K = 3.125 \cdot 10^3$ J/m$^3$, intralayer exchange constant $J_{ex} = 1 \cdot 10^{-11}$ J/m.

Dimensions of platform **II** for modeling were $1500 \cdot 1500$ nm, and the sampling cell dimensions were $5 \times 5 \times 0.3$ nm. The calculations used saturation magnetizations of the top layer $M_{st}$ and bottom layer $M_{sb}$, magnetocrystalline anisotropy constants of the top layer $K_{vt}$ and bottom layer $K_{vb}$, intralayer exchange constant $J_{ex}$ and interlayer exchange constants $J_{af}$. The values were calculated in accordance with the macrospin theory [10] and corrected using the experimental hysteresis loop parameters. The numerical values of these parameters are: $M_{st} = 700$ emu/cm$^3$, $M_{sb} = 1200$ emu/cm$^3$, $K_{vt} = 2 \cdot 10^3$ J/m$^3$, $K_{vb} = 2.5 \cdot 10^3$ J/m$^3$, $J_{ex} = 1.3 \cdot 10^{-11}$ J/m, $J_{af} = -0.73 \cdot 10^{-5}$ J/m$^2$. External field for modeling was 100 Oe as in real experiments.

The initial start state of the systems was taken as follows: single-layer platform **I** magnetized upwards, double-layer platform **II** magnetized into the antiparallel state $\uparrow\downarrow$. Magnetization of both platforms is perpendicular to the film plane. Nanoparticles will be characterized by the saturation magnetization: $M_s = 95\,\mathrm{A} \cdot \mathrm{m}^2/\mathrm{kg}$; nanoparticles interact with each other through the dipole-dipole interaction. In this case this interaction is neglected and the particle is treated as an isolated one, this may be done in case of low concentrations that are generally sought for in devices for detecting magnetic nanoparticles. The particle is taken as a uniformly magnetized sphere with a radius of $R_{par} = 280$ nm, whose magnetization is oriented along the $z$ axis.

A point of contact between the spherical particle and platform is taken as the origin (in Figure 1 the particle is lifted a little above the platform surface for clarity). The uniformly magnetized sphere was described by the point dipole equation with its center in the center of the sphere:

$$\mathbf{H}(\mathbf{p_m}, \mathbf{r}) = \frac{1}{4\pi}\left[\frac{3(\mathbf{p_m}, \mathbf{r})\mathbf{r}}{|\mathbf{r}|^5} - \frac{\mathbf{p_m}}{|\mathbf{r}|^3}\right],$$

where $\mathbf{r}$ is the vector oriented from the center of the particle to the given point P on the platform, $\mathbf{p_m}$ is the magnetic moment of the nanoparticle. $R_{part}$ is the particle radius, $h_{add}$ is the additional nanoparticle lifting height above the platform surface (composed of the thickness of the MgO coating layer), $m$ is the absolute magnetic moment of the particle, $\mathbf{p_m} = (0, 0, -m)$ is the magnetic moment of the particle, $\mathbf{r_0} = (x, y, z)$ is the radius vector of the given point P on the platform, $\mathbf{r_{part}} = (x_{part}, y_{part}, z_{part})$ are the coordinates of the center of cluster in the system of coordinates. Radius vector from the particle center to point P has the coordinates $\mathbf{r} = \mathbf{r_0} - \mathbf{r_{part}} = (x - x_{part}, y - y_{part}, z - z_{part})$. Magnetic moment of the particle has the coordinates $\mathbf{p_m} = (0, 0, -m)$, where $m$ is the absolute magnetic moment. Scalar product $\mathbf{p_m}$ and $\mathbf{r}$ is equal to $(\mathbf{p_m}, \mathbf{r}) = -m(z - z_{part})$.

Expressions for particle field projections on the coordinate axes:

$$H_x(\mathbf{r}, \mathbf{p_m}, x, z, R_{part}, h_{add}) = \frac{-3}{4\pi|\mathbf{r}|^5}\, m\big(z - (R_{part} + h_{add})\big)x$$

$$H_y(\mathbf{r}, \mathbf{p_m}, y, z, R_{part}, h_{add}) = \frac{-3}{4\pi|\mathbf{r}|^5}\, m\big(z - (R_{part} + h_{add})\big)y$$

$$H_y(\mathbf{r}, \mathbf{p_m}, z, R_{part}, h_{add}) = \frac{-m}{4\pi|\mathbf{r}|^5}\left(3\big(z - (R_{part} + h_{add})\big)^2 - r^2\right)$$

$$H_{Zeem}(t_t, t_b, H, \theta_t, \theta_b, M_{st}, M_{sb}) = -\mu_0 H(t_t M_{st}\cos(\theta_t) + t_b M_{sb}\cos(\theta_b)).$$

Heterostructure magnetization is generally affected by: anisotropy $E_{aniz}$, interlayer exchange interaction $E_{af}$ and Zeeman energy $E_{zeem}$:

$$E_{aniz}(\theta_t, K_{st}, \theta_b, K_{sb}) = -K_{st}\cos(\theta_t)^2 - K_{sb}\cos(\theta_b)^2$$

$$E_{af}(J_{af}, \theta_t, \theta_b) = -J_{af}\cos(\theta_t - \theta_b)$$

$$E_{Zeem}(t_t, t_b, H, \theta_t, \theta_b, M_{st}, M_{sb}) = -\mu_0 H(t_t M_{st}\cos(\theta_t) + t_b M_{sb}\cos(\theta_b)),$$

where $\theta_t$ and $\theta_b$ are the angles between magnetization vectors of the top layer$\mathbf{M_t}$ and bottom layer $\mathbf{M_b}$ and platform plane **II**.

## 3. Results and discussion

Surface morphology and magnetic force gradient distribution on the sample surface were studied by the atomic force microscopy (AFM) and magnetic force microscopy (MFM) methods, respectively. Magnetic relief images of platform **II** with particles deposited on its surface are shown in Figure 2. On all fragments of the surface, it can be seen that the sizes of particles or groups of particles in the atomic force microscope (left column) are smaller than the corresponding images in the magnetic force microscope (right column). In [6], it was proved that increase in the dimensions of the „magnetic image“ compared with the original particle size was caused by remagnetization of the ferromagnetic film under the particle. Consequently, the ferromagnetic particle field switches the heterostructure state from the initial $\uparrow\downarrow$ state to one of the $\uparrow\uparrow$, $\downarrow\uparrow$, $\downarrow\downarrow$ states. These four $\uparrow\uparrow$, $\uparrow\downarrow$, $\downarrow\uparrow$, $\downarrow\downarrow$ states can be easily identified on the magnetic hysteresis loop (Figure 3) that contains four magnetic moment levels. They are also denoted in literature as P+, AP+, AP−, P−, respectively. It is reasonable to assume that the magnetic field of particles switches the heterostructure into the nearest energy state $\uparrow\downarrow$. Nanoparticles often are aggregated into much larger assemblies than the particles themselves. In Figure 2,

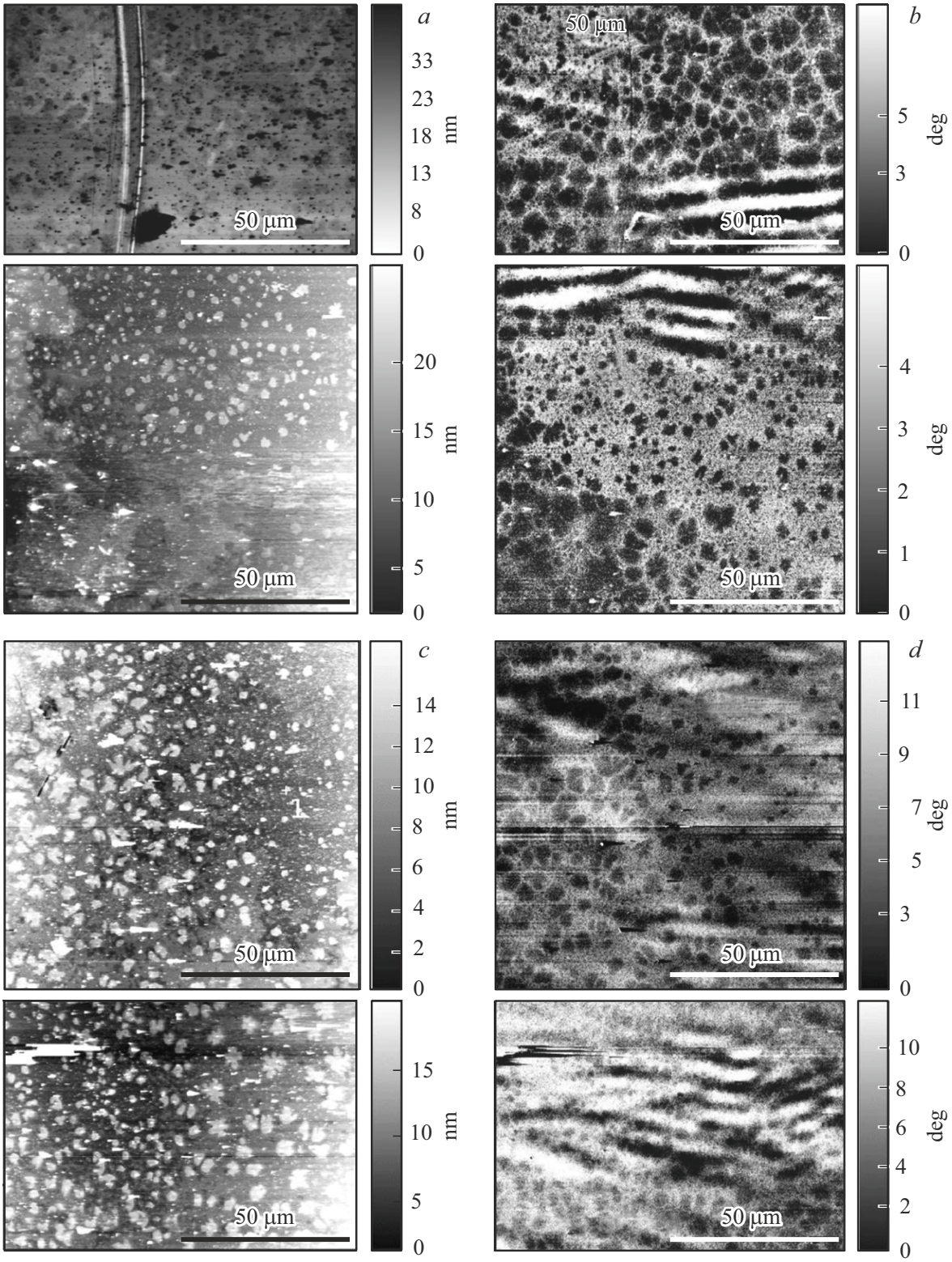


**Figure 2.** Two-dimensional images of the $Fe/Fe_3O_4$ nanoparticles on the CoFeB/Ta/CoFeB platform recorded in the AFM $(a, c, e, g)$ and MFM $(b, d, f, h)$ modes.

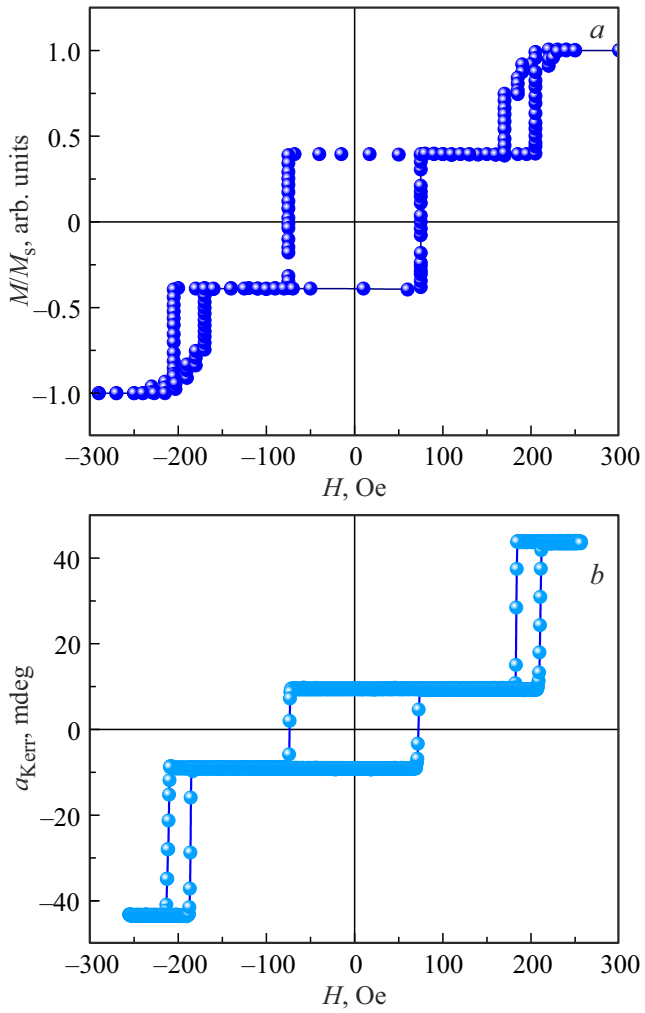


**Figure 3.** (*a*) Modeling of the MgO/CoFeB/Ta/CoFeB/MgO/Ta loop without nanoparticles at $T = 300$ K using OOMMF. (*b*) Experimentally measured specified magnetization hysteresis loop of the MgO/CoFeB/Ta/CoFeB/MgO/Ta sample without nanoparticles at $T = 300$ K using the Kerr microscope. In both cases, the magnetic field was applied along the normal to the sample plane.

particle sizes are much larger that those of nanoparticles. The mean size of 280 nm was used for modeling.

For modeling, state switching fields and magnetization levels typical of each of the four states were obtained from the hysteresis loop (Figure 3). Such selection of parameters that could provide quantitative similarity of the experimental hysteresis loop (Figure 3, *a*) with the hysteresis loop recorded using the Kerr microscope (Figure 3, *b*) was used as a start point for modeling. After completion of hysteresis loop fitting, distributions of single-layer magnetization induced by the $Fe/Fe_3O_4$ particles were plotted. Modeling results for platform **I** are shown in Figure 4. Magnetization in a single CoFeB thin film of sample **I** is defined by the anisotropy energy and Zeeman energy. When the field is oriented perpendicularly to the film, non-monotonic magnetization distribution associated with combination of the external field and magnetic dipole (particle) field can be seen Figure 4, *a*. Far away from the particle, layer magnetization is similar everywhere at the film saturation magnetization level 950 emu/cm$^3$. In areas close to the particle center, magnetization reduction is observed initially due to the external field compensation by the dipole field. In the center, magnetization return to the value that takes place faraway from the particle.

Figure 4, *b*–*d* shows magnetization distributions when the external magnetic field is applied at non-zero angles to normal of a single film. Magnetization distribution asymmetry induced by field deviation from normal is reasonable to expect. When the field direction with respect to platform **I** is changed, the platform magnetization is redirected such that the magnetic dipole axis gets slightly deviated from normal to the film approaching the film surface.

Figure 5 shows design distributions of the magnetization projections on the vertical axis for the top layer $M_{tz}$ (left column with figures) and bottom layer $M_{bz}$ (right column of figures) of CoFeB platform **II** under the nanoparticle cluster with a radius of 280 nm in the 100 Oe external field at the angles between the field and normal to films $\theta = 0°$ (*a, b*), $\theta = 30°$ (*c, d*), $\theta = 60°$ (*e,f*) and $\theta = 90°$ (*g, h*). In the field perpendicular to the film, the top layer far from the particle is magnetized opposite to the field (strong background) (Figure 5, *a*), and the bottom layer is magnetized along the field (red background in Figure 5, *b*). This corresponds to the initial magnetization state in this external field (without the particle) AP+. Near the particle, the top layer is remagnetized along the field (Figure 5, *a*), and the bottom layer has a non-monotonic magnetization distribution with decreased values not far away from the particle center and with the maximum under the particle center (Figure 5, *b*). With deviation of the external magnetic field from normal, the central magnetization peak of the top film is split into the maximum and minimum, the presence of which means that there is a magnetic dipole moment projection on the XY plane (Figure 5, *d*). Positive magnetization peak of the bottom film becomes asymmetric (Figure 5, *c*). In other words, the magnetic dipole lying in the film plane is formed by the negative pole of the bottom film and the positive poles of the top film at $\theta = 90°$ (Figure 5, *e*–*h*).

Thus, in a single-layer film, the field perpendicular to the spontaneous film magnetization doesn't reverse the magnetization into the film plane, but just slightly deviates it. In a double-layer structure, where one of the films is the same as in a single-layer structure, reversal of the total magnetic moment to the film plane is observed in the same magnetic field oriented along the film. Negative and positive dipole magnetization areas with the axis lying in the plane are observed in different planes — top and bottom. Therefore, the presence of exchange-coupled ferromagnetic film has such effect on the initial ferromagnetic layer that is equivalent to a decrease in the effective anisotropy.

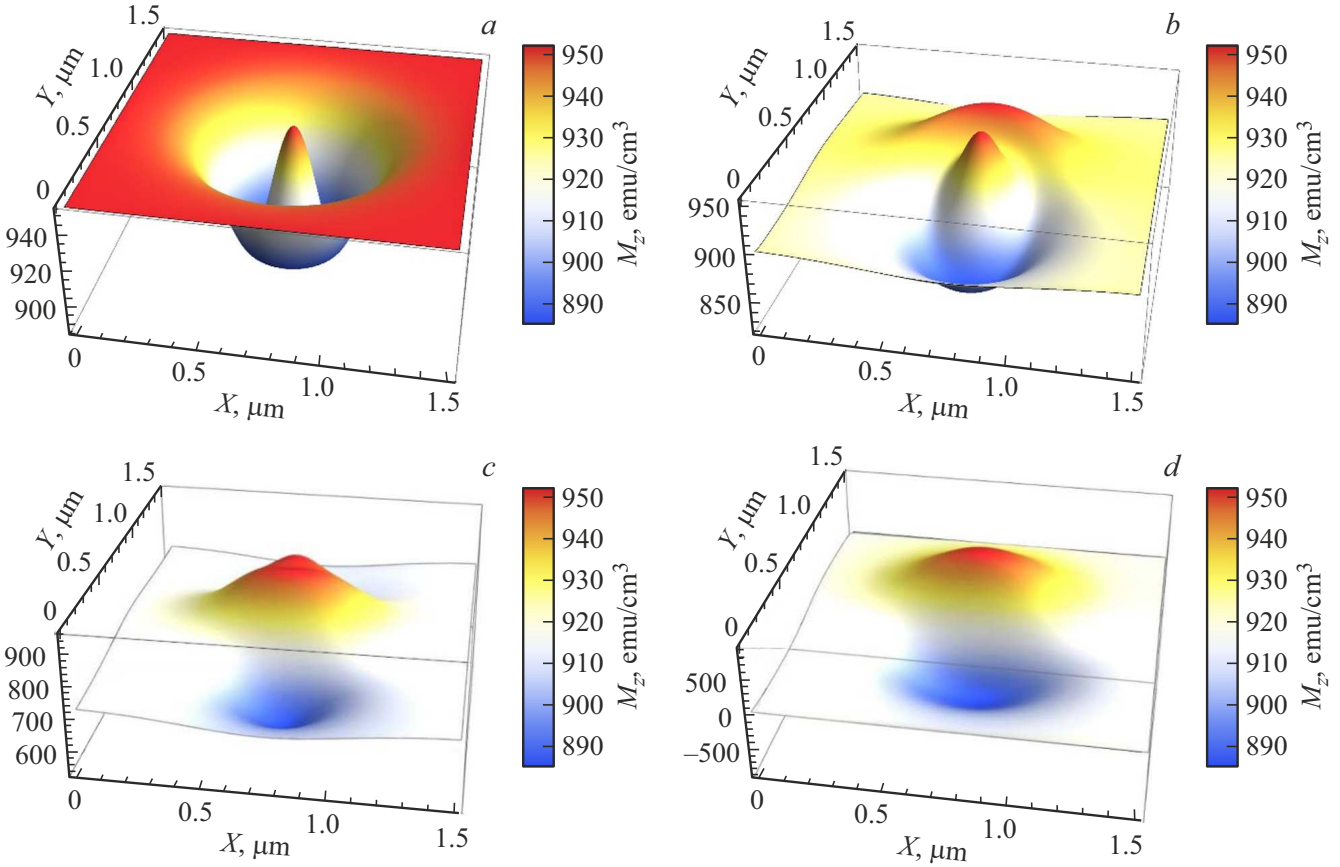


**Figure 4.** Magnetization projection distribution of the ferromagnetic layer of CoFeB platform **I** exposed to the external uniform field **H** with a strength of 100 Oe and scattering field $\mathbf{H}_{dip}$ of the cluster with a radius of 280 nm for various angles between the external field and normal to the sample $\theta = 0^\circ$ (*a*), $\theta = 30^\circ$ (*b*), $\theta = 60^\circ$ (*c*), $\theta = 90^\circ$ (*d*).

Note that magnetic images (magnified compared with the initial particle size) of particles on the heterostructure surface (Figure 2) were recorded as a result of cantilever attraction by the field oriented perpendicular to the surface. This component is induced by the magnetic dipole with the axis perpendicular to the surface, i.e. (for example, in a single film(Figure 4, *d*)).

Modeling of the remagnetized area of platform **I** for different radii if particles on the surface is shown in Figure 6. It can be seen that the dimensions of the area remagnetized by the magnetic field of the particle grow as its radius increases. But there are no qualitative changes in the film magnetization distribution as the particle sizes grow.

Similar calculations were performed for other particle radii and for a double-layer heterostructure. Remagnetized area size $R_n$ was determined as shown in Figure 7 by arrows for various types of remagnetization.

Results of these calculations are summarized in Figure 8 that shows calculated dependences of the radius of the remagnetized film area $R_n$ on the particle radius $R$ for the CoFeB monolayer and for the bottom layer of the CoFeB/Ta/CoFeB platform as well as or the top layer of platform **II**. It can be seen that at small particle radii the remagnetized area on the film is just a little larger than the particle size, while at large particle radii ($\sim 150\,\mu$m) the remagnetized area on the film is twice as large as the particle radius.

Thus, bilayer platforms respond to the scattering field of submicron ferromagnetic particles such that the dimensions of the remagnetized areas are much greater than the particle sizes, i.e. a real coefficient connecting the particle concentration and magnetoresistance that can be used to record particles turns to be n-fold higher than the expected one. Such platforms are response „amplifiers“ in the particle field–magnetoresistance system. Note that this fact can also lead to a situation when evaluation of the number of particles, whose concentration on the platform is high, from the magnetoresistance signal might be incorrect due to overlapping of the remagnetized areas.

The CoFeB/Ta/CoFeB platforms studied in this work show the giant magnetoresistance (GMR) effect. They may be used for detection and quantitative assessment of magnetic microparticles and nanoparticles on their surface, which has a significant potential in biomedical applications such as diagnosis of diseases, drug delivery and biomarker detection. When a magnetic particle GMR sensor is placed on the surface, they change local magnetization

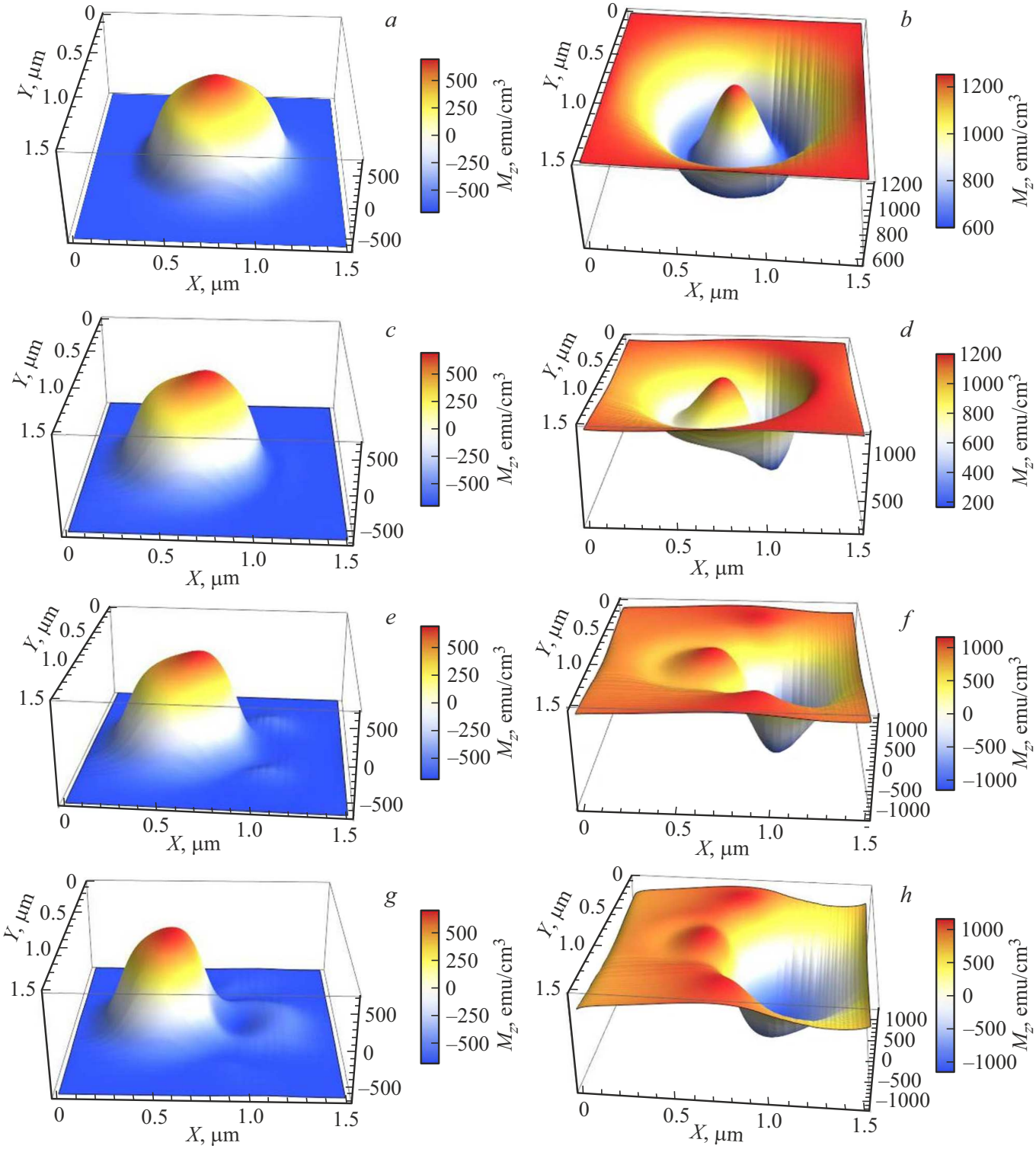


**Figure 5.** Magnetization projection distribution of the top layer $\boldsymbol{M}_{\mathbf{tz}}$ (left column *a, c, e, g*) and bottom layer $\boldsymbol{M}_{\mathbf{bz}}$ (right column *b, d, f, h*) to normal of MgO/CoFeB/Ta/CoFeB/MgO/Ta platform **II** under the nanoparticle cluster with a radius of 280 nm in the 100 Oe external field at the angles between the field and normal to films $\theta = 0^\circ$ (*a, b*), $\theta = 30^\circ$ (*c, d*), $\theta = 60^\circ$ (*e, f*) and $\theta = 90^\circ$ (*g, h*).

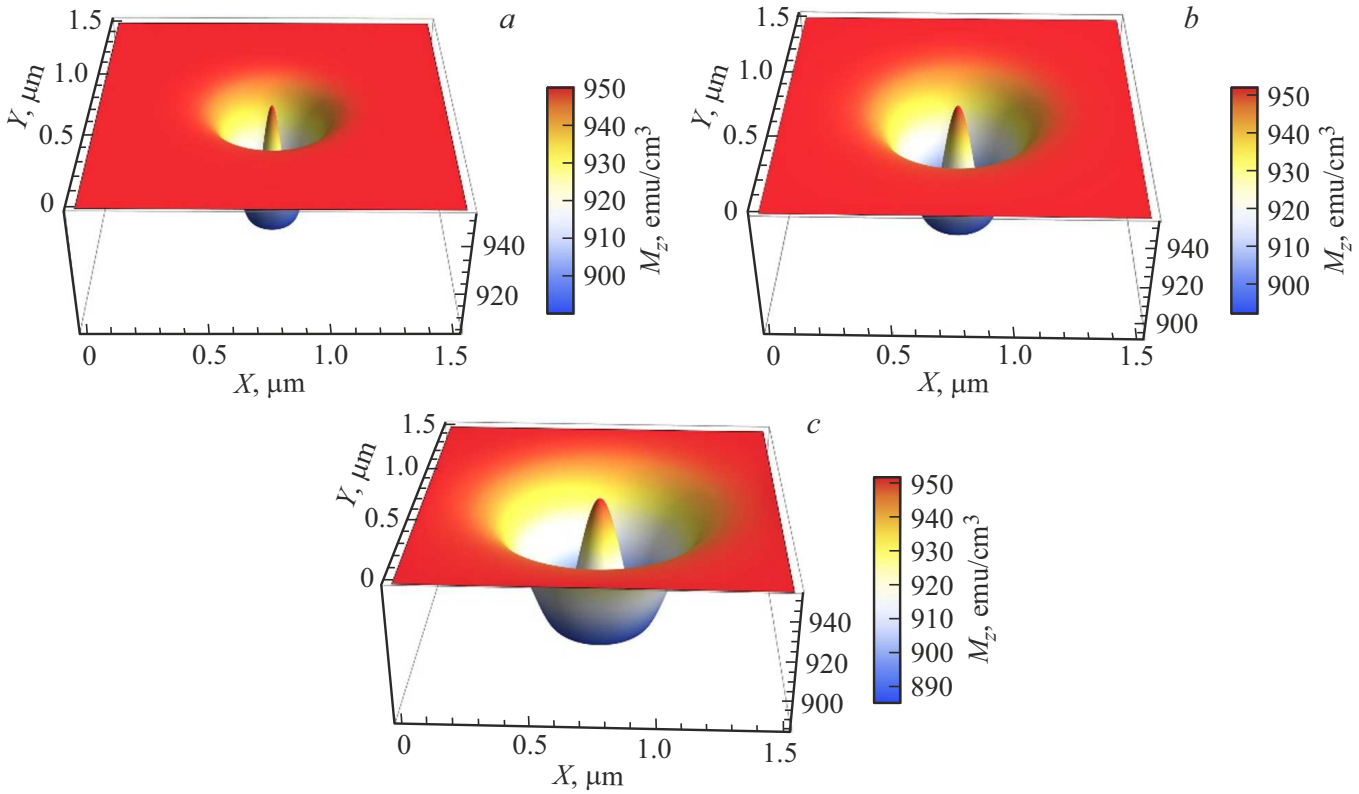


**Figure 6.** Magnetization distribution of the CoFeB platform (monolayer) exposed to the scattering field of the particle with radii: 140 (*a*), 200 (*b*), 280 (*c*) nm.

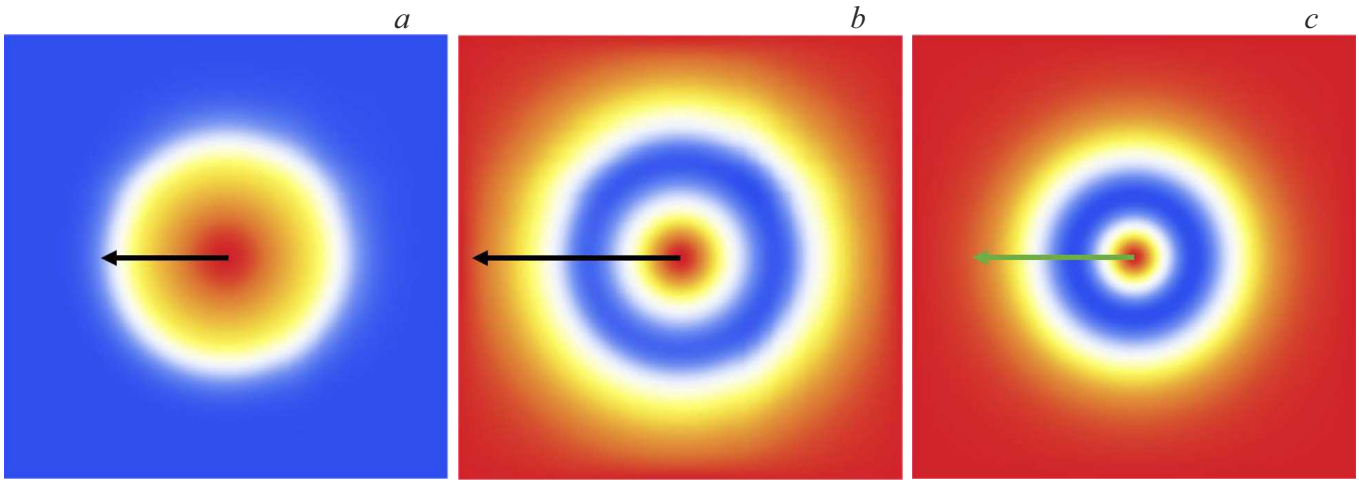


**Figure 7.** magnetization distribution of the top layer (*a*) and bottom layer (*b*) of platform **II**: and platform **I** (*c*) exposed to the scattering field of the particle with a radius of 280 nm. Arrows show the radius of the maximum area involved in the remagnetization $R_n$.

of ferromagnetic layers. These local changes lead to a change in the sensor magnetoresistance which can be later determined by measuring the voltage-current characteristics of GMR sensors integrated into microfluid platforms [11,12]. Correlation between the changes in the magnetoresistance and particle concentration provides accurate quantitative assessment.

## 4. Conclusions

Micromagnetic modeling (OOMMF) was used to visualize remagnetization of a ferromagnetic thin film (CoFeB) and heterostructure consisting of two ferromagnetic layers separated by a nonmagnetic material (CoFeB/Ta/CoFeB) exposed to a ferromagnetic nanoparticle on its surface. It

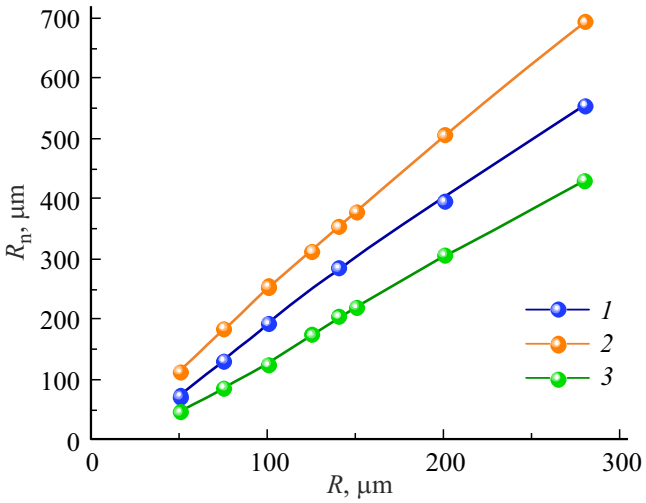


**Figure 8.** Dependence of the area radius involved in the remagnetization $R_n$ on the particle radius $R$ for the CoFeB monolayer (*1*), bottom layer of CoFeB/Ta/CoFeB platform **II** (*2*), top layer of CoFeB/Ta/CoFeB platform **II** (*3*).

was found that the field lying in the structure plane didn't reverse the magnetization of a single film into the plane, but did that in a heterostructure, in which an exchange-coupled film was added to a film whose parameters were the same as those of a single film. Remagnetization area in a heterostructure (CoFeB/Ta/CoFeB) is larger than that in a monolayer (CoFeB). Remagnetized area size grows quasi linearly as the particle size grows, and the difference between the particle size and remagnetized area size grows with particle size.

The modeling results are of interest for measuring concentration of nanoparticles or magnetolabeled objects deposited on the ferromagnetic sensor surface.

## Funding

E.I. Kunitsyna was supported by the grant provided by the Russian Science Foundation No. 24-72-00049, https://rscf.ru/project/24-72-00049/, R.B. Morgunov was supported by a thematic map of the Federal Research Center of Problems of Chemical Physics and Medicinal Chemistry RAS 124020700089-3.

## Conflict of interest

The authors declare the absence of conflicts of interest.

## References

[1] X. Zhi, M. Deng, H. Yang, G. Gao, K. Wang, H. Fu, Y. Zhang, D. Chen, D. Cui. Biosens. Bioelectron. **54**, 372 (2014). https://doi.org/10.1016/j.bios.2013.11.025
[2] P. Zhang, N. Thiyagarajah, S. Bae. IEEE Sens. J. **11**, *9*, 1927 (2011). https://doi.org/10.1109/JSEN.2010.2102349
[3] P.P. Freitas, F.A. Cardoso, V.C. Martins, S.A.M. Martins, J. Loureiro, J. Amaral, R.C. Chaves, S. Cardoso, L.P. Fonseca, A.M. Sebastião, M. Pannetier-Lecoeur, C. Fermon. Lab Chip **12**, *3*, 546 (2012). https://doi.org/10.1039/c1lc20791a
[4] A. Kaidatzis, D.B. Gopman, C. Bran, J.M. García-Martín, M. Vázquez, D. Niarchos. J. Magn. Magn. Mater. **473**, 355 (2019). https://doi.org/10.1016/j.jmmm.2018.10.103
[5] O.V. Koplak, E.I. Kunitsyna, R.S. Allayarov, S. Mangin, N.V. Granovskii, R.B. Morgunov. J. Exp. Theor. Phys. **131**, *4*, 607 (2020). https://doi.org/10.1134/S1063776120090046
[6] R.B. Morgunov, O.V. Koplak, R.S. Allayarov, E.I. Kunitsyna, S. Mangin. Appl. Surf. Sci. **527**, 146836 (2020). https://doi.org/10.1016/j.apsusc.2020.146836
[7] O. Koplak, A. Talantsev, Y. Lu, A. Hamadeh, P. Pirro, T. Hauet, R. Morgunov, S. Mangin. J. Magn. Magn. Mater. **433**, 91 (2017). https://doi.org/10.1016/j.jmmm.2017.02.047
[8] T. Fache, H.S. Tarazona, J. Liu, G. L'Vova, M.J. Applegate, J.C. Rojas-Sanchez, S. Petit-Watelot, C.V. Landauro, J. Quispe-Marcatoma, R. Morgunov, C.H.W. Barnes, S. Mangin. Phys. Rev. B **98**, *6*, 1 (2018). https://doi.org/10.1103/PhysRevB.98.064410
[9] R.B. Morgunov, G.L. L'vova, A.D. Talantsev, O.V. Koplak, T. Fache, S. Mangin. J. Magn. Magn. Mater. **459**, 33 (2018). https://doi.org/10.1016/j.jmmm.2017.12.083
[10] R. Morgunov, Y. Lu, M. Lavanant, T. Fache, X. Deveaux, S. Migot, O. Koplak, A. Talantsev, S. Mangin. Phys. Rev. B **96**, *5*, 1 (2017) https://doi.org/10.1103/PhysRevB.96.054421
[11] J. Devkota, G. Kokkinis, T. Berris, M. Jamalieh, S. Cardoso, F. Cardoso, H. Srikanth, M.H. Phan, I. Giouroudi. RSC Adv. **5**, *63*, 51169 (2015). https://doi.org/10.1039/c5ra09365a
[12] T.R. Ger, P.S. Wu, W.J. Wang, C.A. Chen, P.A.R. Abu, S.L. Chen. Biosensors **13**, *8*, 1 (2023). https://doi.org/10.3390/bios13080807

*Translated by E.Ilinskaya*